Molecular beacon-decorated Polymethylmethacrylate Core-shell Fluorescent Nanoparticles for the Detection of Survivin mRNA in Human Cancer Cells

Barbara Adinolfi[a]*, Mario Pellegrino[b], Ambra Giannetti[a], Sara Tombelli[a], Cosimo Trono[a], Giovanna Sotgiu[c], Greta Varchi[c], Marco Ballestri[c], Tamara Posati[c], Sara Carpi[d], Paola Nieri[d‡], Francesco Baldini[a‡]

[a]Istituto di Fisica Applicata "Nello Carrara", Consiglio Nazionale delle Ricerche, Via Madonna del Piano 10, 50019, Sesto Fiorentino (Fi), Italye-mail address: b.adinolfi@ifac.cnr.it; a.giannetti@ifac.cnr.it; s.tombelli@ifac.cnr.it; c.trono@ifac.cnr.it; f.baldini@ifac.cnr.it[b]Dipartimento di Ricerca Traslazionale e delle Nuove Tecnologie in Medicina e Chirurgia, Università di Pisa, Via Savi 10, 56126, Pisa, Italye-mail address: mario.pellegrino@unipi.it[c]Istituto per la Sintesi Organica e la Fotoreattività, Consiglio Nazionale delle Ricerche, Via P. Gobetti 101, 40129, Bologna, Italye-mail address: giovanna.sotgiu@isof.cnr.it; greta.varchi@isof.cnr.it; marco.ballestri@isof.cnr.it; tamara.posati@isof.cnr.it[d]Dipartimento di Farmacia, Università di Pisa, Via Bonanno Pisano 6, 56126, Pisa, Italy e-mail address: sara.carpi@for.unipi.it; paola.nieri@farm.unipi.it

‡These authors contributed equally to this work.

*Corresponding author:

Barbara Adinolfi

Istituto di Fisica Applicata "Nello Carrara", Consiglio Nazionale delle Ricerche, Via Madonna del Piano 10, 50019, Sesto Fiorentino (Fi), Italy

e-mail address: b.adinolfi@ifac.cnr.it phone number: +39 055 5226359

fax number: +39 055 5226400

Abstract

One of the main goals of nanomedicine in cancer is the development of effective drug delivery systems, primarily nanoparticles.

Survivin, an overexpressed anti-apoptotic protein in cancer, represents a pharmacological target for therapy and a Molecular Beacon (MB) specific for survivin mRNA is available. In this study, the ability of polymethylmethacrylate nanoparticles (PMMA-NPs) to promote survivin MB uptake in human A549 cells was investigated.

Fluorescent and positively charged core PMMA-NPs of nearly 60 nm, obtained through an emulsion co-polymerization reaction, and the MB alone were evaluated in solution, for their analytical characterization; then, the MB specificity and functionality were verified after adsorption onto the PMMA-NPs.

The carrier ability of PMMA-NPs in A549 was examined by confocal microscopy. With the optimized protocol, a hardly detectable fluorescent signal was obtained after incubation of the cells with the MB alone (fluorescent spots *per* cell of 1.90 ± 0.40 with a mean area of 1.04 ± 0.20 μm^2), while bright fluorescent spots inside the cells were evident by using the MB loaded onto the PMMA-NPs. (27.50 ± 2.30 fluorescent spots *per* cell with a mean area of 2.35 ± 0.16 μm^2). These results demonstrate the ability of the PMMA-NPs to promote the survivin-MB internalization, suggesting that this complex might represent a promising strategy for intracellular sensing and for the reduction of cancer cell proliferation.

Keywords: Core-shell Polymethylmethacrylate Nanoparticles; Molecular Beacon; survivin; cellular up-take; A549 human lung adenocarcinoma epithelial cells; sensing in cell

1. Introduction

Effective drug delivery into cancer cells is a major objective for nanomedicine, which exploits the peculiar characteristics of cancer tissues, such as their enhanced permeability and retention (EPR) properties (Kobayashi et al., 2014). As delivery vehicles of anticancer drugs, nanoparticles (NPs) offer numerous advantages over conventional drug delivery approaches, such as the possibility of multiple functionalization for improving the imaging, diagnosis and targeted therapy (Ashley et al., 2012; Biswas et al., 2014; Bogart et al., 2014; Guo et al, 2015; Hardy et al., 2015). Moreover, NPs can enhance active or passive targeting and thus increase selectivity, reduce toxicity and prolong the drug half-life in the human body with respect to the free drug (Kim et al., 2014; Lee et al., 2014; Wang et al., 2014).

The size, stability and surface properties of NPs greatly affect the efficiency of their biological activity and their capping agents largely influence these characteristics (Kejlová et al., 2015; Maurizi et al., 2015). Moreover, surface NP charge plays an important role on their interactions with cell surface (Li et al., 2015; Maurizi, et al., 2015) and it has been demonstrated that cationic particles generally exert stronger effect on cellular uptake (Frohlich 2012; Li et al., 2015).

It has been shown that several types of drugs can be loaded onto NPs by different approaches: a) incorporation into the NP core, either by cleavable covalent bonds or by hydrophobic interactions (Gao et al., 2006); b) covalently bonded on the surface through a cleavable linker (Sun et al., 2014); c) electrostatically loaded on the external shell (Monasterolo 2012). Among these loading methodologies, covalent bonding requires higher energy to complete the heterogeneous chemical reaction between the bioactive molecules and the matrices and it needs the presence of functional groups to achieve covalent bond formation. In contrast, the NPs-electrostatic loading needs less energy for the combination with the drug, and it occurs by simple mixing of the two components generally leading to a higher loading ratio (Varchi 2015).

To improve the sensing imaging in cancer, a strategy consists in the encapsulation of organic dyes into nano-matrices, providing higher fluorophore photo-stability. Another important advantage is the superior brightness of this nano-complex, which is due to the higher number of dye molecules loaded on one nanoparticle (Monasterolo 2012).

In particular, the core-shell polymethylmethacrylate nanoparticles (PMMA-NPs) used in this study consist of a hydrophobic PMMA core covalently functionalized with fluorescein and an external hydrophilic shell decorated with primary amine groups and quaternary ammonium salts. PMMA-NPs have high biocompatibility, very low cytotoxicity, biological inertness, low costs of synthesis. Furthermore, the possibility of multiple functionalization for improving the selectivity and the ability to prolong the drug half-life in the human body with respect to the free drug (Kim et al., 2014; Lee et al., 2014; Wang et al., 2014; Bettencourt and Almeida, 2012) represent relevant advantages with respect to classical transfection reagents such as Lipofectamine. In addition, although Lipofectamine generally provides good/high transfection efficiency promoting DNA penetration through intact nuclear envelopes without excessive cytotoxicity, besides which it is easy to use and minimal steps for the transfection are required, it was demonstrated and is widely recognized that its use is not applicable to all cell types (Dalby et al., 2004); moreover, it is commonly used to introduce nucleic acids in some *in vitro* cellular models (Guo et al., 2016; Teagle et al., 2016; Rawat and Gadgil, 2016; Zhang et al., 2016) but its utilization has not been extended *in vivo*.

PMMA has been approved by the Food and Drug Administration (FDA) for human clinical applications and used successfully in bone cement to fix total joint prostheses (Lou et al, 2007). Moreover, in previous studies it has been demonstrated that similar NPs administered *in vivo* were excreted in feces up to 80% (intraperitoneal administration) or 100% (oral administration), with no significant toxicity for the animals (Falzarano et al., 2014).

Additionally, similar kind of nanoparticles have been previously used as carriers of drugs, prodrugs (Chen et al., 2016; Fraix et al., 2015; Tian et al., 2016) and antisense oligoribonucleotides for inducing dystrophin restoration in body-wide muscles in the X chromosome-linked muscular dystrophy animal model (Ferliniet al., 2010). Moreover, previous studies demonstrated that similar nanoparticles used for drug delivery purposes with different sizes, e.g. 40, 55, 100 and 180 nm, showed comparable ability to cross the cell membrane regardless to their size (Varchi et al., 2015; Varchi et al., 2013). In fact, despite the rate and mechanism of nanoparticles uptake is cell-type dependent and varies among nanoparticles of different size, charge, and other surface properties, it has been reported that cationic particles generally enhance cellular uptake regardless to their size and morphology (Samal et al., 2012).

The idea developed in this work is to use biocompatible core-shell polymethylmethacrylate nanoparticles (PMMA-NPs) as carrier of an oligodeoxynucleotide molecular beacon (MB) specific for survivin mRNA in A549 human lung adenocarcinoma epithelial cells.

Survivin mRNA is considered a promising target for anticancer treatment. Indeed, survivin is a protein belonging to the Inhibitor of Apoptosis Protein family (IAP) that plays a key role in several cellular functions, such as the regulation of cell cycle, apoptosis and cell migration (Brun et al., 2015; Dallaglio et al., 2012; Liu et al., 2014; Wu, et al., 2014).

Furthermore, its expression is very high in most cancer cells (Baran et al., 2009; Mera, et al., 2008) in which the protein levels correlate to poor prognosis and resistance to chemotherapeutic treatment (Schmidt et al., 2003; Sommer et al., 2003), while it is rarely expressed in healthy tissues (Fukuda and Pelus 2006).

Several anticancer therapeutic strategies targeting survivin have been already considered (Beckeret al., 2011), among which the antisense oligonucleotide Gataparsen has successfully reached the phase II clinical trial (Singh et al., 2015).

Molecular beacons (MBs) are potential theranostic agents (Li et al., 2014; Zheng et al., 2015; Wang et al., 2013), acting at the same time as sensors able to detect endogenous nucleic acids, and as drug, by silencing the target RNA (Tay et al., 2015).

A MB is a stem-loop-folded oligodeoxynucleotide with fluorophore and quencher dyes conjugated to the opposite end of the hairpin. In the absence of the complementary nucleic acid target, the fluorescence of the fluorophore is quenched by the closely located quencher (Huang et al., 2014). Otherwise, the hybridization with the target opens the hairpin, generating a probe-analyte duplex that physically separates the fluorophore from the quencher, allowing the emission of a fluorescent signal after excitation (Giannetti et al., 2013; Santangelo et al., 2006).

Carpi and colleagues (2014) have shown in an *in vitro* study on human cutaneous melanoma cell lines that the survivin-MB carried into the cells by lipofectamine was selective for the mRNA target and acted as pro-apoptotic agent. On the basis of this evidence, and in order to both decrease the MB enzymatic degradation that may occur *in* vivo (Teo et al., 2015; Bishop et al., 2015) and to permit the MB delivery also in perspective of an *in vivo* application, we focused our attention on the characterization of the experimental conditions able to guarantee the survivin-MB cellular up-take by using PMMA-NPs as carriers. In fact, the presence of quaternary ammonium salts on the outer shell of the particles, along with the possibility of covalently functionalize their core with properly selected fluorophores, make PMMA-NPs particularly suitable for such application. The pharmacological effects of the MB in terms of reduction of survivin mRNA expression and of induction of apoptosis in A549 cells were not considered in the present work. The study is finalized to examine the MB sensing properties, by means of a thorough investigation of its internalization through the chosen NPs and of its maintained capability to interact with and detect the associated mRNA. This aspect, often underestimated or neglected, is essential and in our opinion constitutes a mandatory step before concentrating on the therapeutic effect."

In this view, we first assessed the most appropriate conditions for PMMA-NPs cell internalization, both in terms of NP concentration and exposure time. In the second phase of the study, we evaluated the behavior of the selected MB when administered to A549 cells as free or loaded onto the NPs. Indeed, as expected, we observed that, when only MB (without NPs) was administered, a poor fluorescent signal was generated, while, by using the MB loaded onto PMMA-NPs, bright fluorescent spots were detectable inside the cells, indicating the ability of PMMA-NPs to promote the survivin-MB internalization.

2. Material and methods

2.1. Survivin molecular beacon

The survivin MB and its reverse sequence were purchased from IBA (Gottingen, Germany) with the following sequence (Nitin et al., 2004):

5'-(ATTO 647N)CGACGGAGAAAGGGCTGCCACGTCG(BBQ)-3'

The underlined sequence represents the specific sequence for survivin mRNA with the ATTO 647N (λ_{abs} 644 nm, λ_{em} 669 nm) and the BBQ650 (λ_{max} ~ 650 nm, useful absorbance between 550 and 750 nm) as fluorophore/quencher pair, covalently bound to its distal ends.

The reverse-MB sequence is:

5'-(ATTO 647N)GCTGCACCGTCGGGAAAGAGGCAGC(BBQ)-3'

The DNA sequence complementary to the MB (target 5'-CCCCTGCCTGGCAGCCCTTTCTCAAGGACC-3') and the DNA non-specific sequence (5'-ATCGGTGCGCTTGTCG-3') were purchased from Twin Helix (Milan, Italy).

RPMI 1640 medium, fetal bovine serum (FBS), penicillin, streptomycin and all the other chemicals, unless otherwise stated, were purchased from Sigma (Milan, Italy).

2.2. Synthesis of PMMA-NPs

Fluorescent PMMA-NPs were obtained using the experimental procedure described as follows. An aqueous solution (100 mL) of 2-(dimethyloctyl) ammonium ethylmethacrylate bromide (1.02 g, 2.93 mmol) was introduced, at room temperature, into a 250 mL three-neck reactor equipped with a condenser, a mechanical stirrer, a thermometer and inlets for nitrogen. The mixture was purged with nitrogen for 10 minutes, at a stirring rate of 300 rpm, and heated to 80 °C.

Then AEMA (2-Aminoethyl methacrylate hydrochloride) (0.60 g, 3.63 mmol) was added. After solubilization, the di-allyl fluorescein derivative (6.67 mg, 0.027 mmol) (Rimessi et al., 2009) dissolved in methylmethacrylate (1.87 g, 18.7 mmol) was added to reaction mixture. After 5 min of equilibration time, 2,2'-azobis(2-methylpropionamidine) dihydrochloride (AIBA) (11.9 mg, 0.044 mmol) dissolved in 1 mL of deionized water, was added and the mixture was allowed to react for 4 h. The product was purified by dialysis to remove residual monomer and stabilizer. NPs were further purified by subsequent washings on a stirred ultrafiltration cell Amicon system (Millipore model 8050) with milliQ water (100 kDa filters; 5 x). The use of the two selected positively charged co-monomers allows the synthesis of nanoparticles decorated with both quaternary ammonium salts, which are exploited for the electrostatic binding with negatively charged molecules, and primary ammonium salts, which could be in principle used for post-functionalization with targeting antennas for selective delivery to the tumor tissue.

2.3. Characterization of PMMA-NPs

PMMA-NPs UV spectra were determined by spectrophotometric measurement with a Lambda 20 Perkin Elmer spectrophotometer (Waltham, MA, USA). The hydrodynamic diameter of the nanoparticles (Table S1) was determined by photon correlation spectroscopy (PCS) at 25 °C using a NanoBrook Omni Particle Size Analyzer (Brookhaven Instruments Corporation, USA) equipped with a 35 mW red diode laser (nominal 640 nm wavelength). As

far as the electrophoretic mobility is concerned, ζ-potential was measured at 25 °C by means of the same system (Table S2). The loading per gram of nanoparticles of primary and quaternary ammonium groups was determined by potentiometric titration of the chloride and bromide ions, respectively obtained after complete ion exchange. The ionic exchange was accomplished by dispersing 10.8 mg of the nanoparticles sample in 25 mL of 1 M KNO_3 at room temperature for 30 min. The mixture was then adjusted to pH 2 with dilute H_2SO_4 and bromide and chloride ions were titrated with a 0.0201 M solution of $AgNO_3$. The samples for the atomic force microscopy (AFM) measurements were prepared by spin-coating deposition of 1 mL of NPs (1 mg mL^{-1}) on atomic flat silicon substrate at 1500 rpm. These experimental conditions allow to prevent the aggregation of the nanoparticles and to obtain a uniform deposition over 1 cm^2 of isolated nanoparticles, which can be clearly distinguished from the substrate. AFM topographical images were collected using an NT-MDT (Italy) solver scanning probe microscope in tapping mode. Particles morphology was further studied using the EVO LS 10 LaB6 scanning electron microscopy (SEM) (Zeiss, Italy) with an acceleration voltage of 5 kV and a working distance of 5 mm. The samples were sputter coated under vacuum with a thin layer (10–30 Å) of gold.

2.4. Fluorescence measurement setup

Fluorescence measurements were carried out in a cuvette (Eppendorf UVette®, Eppendorf, Milan, Italy) by using, for excitation, a PicoQuant LDH-P-C-635B laser diode emitting at 635 nm, filtered by means of bandpass interference filters ThorLabs FL635-10 (central wavelength: 635 nm; bandwidth: 10 nm FWHM), and a Nichia NDS1113E laser diode emitting at 485 nm, filtered by means of an interference band pass optical filter Andover 488FS10 (central wavelength: 488 nm; bandwidth: 10 nm FWHM). The emitted fluorescence was collected by means of a multimode optical fiber coupled with a GRIN lens, filtered by means of an interference long-pass optical filter Thorlabs FEL0650 (cut-on wavelength: 650

nm) and an interference long-pass optical filter Semrock BLP01-488R-25 (cut-on wavelength: 500 nm), for the analysis at 635 nm and 485 nm respectively, and detected on an optical spectrometer Andor Shamrock 303i.

2.5. Cell culture and cell viability assay

A549 human lung adenocarcinoma epithelial cells and primary human dermal fibroblasts isolated from adult skin (HDFa) were cultured as reported in the Supplementary material.

Cell viability was measured by using a method based on the cleavage of the 4-(3-(4-iodophenyl)-2-(4-nitrophenyl)-2H-5-tetrazolio)-1,3-benzene disulfonate (WST-1) to formazan by mitochondrial dehydrogenase by following the protocol reported in the Supplementary material.

2.6. Confocal imaging and cellular uptake studies

Laser scanning confocal microscopy was carried out by using a microscope Radiance Plus (Bio-Rad, Milan, Italy) mounted on a Nikon Diaphot inverted microscope. All observations were made with a Nikon oil immersion objective 40X (NA=1.3).

Briefly, A549 cells were plated at 10% of confluence on 35 mm µ-dishes (Ibidi Giemme Snc, Milan, Italy) in complete medium and, after 24 h, incubated with 10 µg mL^{-1} PMMA-NPs (the concentration was chosen on the basis of the cell viability results) or with 100 nM MB or with the MB loaded onto PMMA-NPs. The MB@PMMA-NPs mix was obtained by leaving 100 nM of MB in contact with 10 µg mL^{-1} of NPs for 3 minutes in RPMI 1640 complete medium. After the treatment and three washes (800 µL/each) in PBS buffer, the cells were observed by confocal microscopy in complete medium.

The suitable experimental conditions to ensure the NPs cellular uptake were assessed by using the PMMA-NPs alone in complete medium. Then, the MB alone and the MB loaded onto NPs were tested by using the same protocol.

The protocol for the MB@PMMA-NPs cellular uptake studies in HDFa cells was the same used for A549 cells. Briefly, HDFa cells were plated on 35 mm µ-dishes in complete medium and treated with 10 µg mL^{-1} PMMA-NPs coupled with 100 nM MB for 90 minutes.

Fluorescence images were collected at different time points (from 10 min up to 48 h) of incubation and in two different optical configurations: 1) excitation at 488 nm with an Argon ion laser without any excitation filter and fluorescence collection with an emission filter centered at 530 nm and characterized by a 60 nm bandwidth, for the imaging of fluorescein-doped PMMA nanoparticles; 2) excitation at 638 nm with a laser diode without any excitation filter and fluorescence collection with a long pass emission filter having the cut-on wavelength at 660 nm, for the imaging of the Atto647N/BBQ650 labeled MB.

Data were collected as stacks of images acquired at Z steps of 0.5 µm and including single entire cells.

Acquired images were processed using the MedNuc Ortwiew or 3D Volume Viewer plugin of the open source ImageJ software. NPs or MB fluorescent spots at different times of incubation were localized in equatorial sections of each Z stack with the support of the relative XZ and YZ projections.

3. Results and discussion

3.1. PMMA-NPs synthesis and characterization

Fluorescent core-shell PMMA nanoparticles, (Figure 1A), were obtained by emulsion co-polymerization reaction: during the polymerization all the reagents concur to form an initial micelle where hydrophobic chains locate inside the micelle (core), while the hydrophilic ones, e.g. chains bearing the quaternary and primary ammonium salts, remain in the external water phase (shell) (Chaudhuri and Paria, 2012; Kumar et al., 2013). The NPs were characterized by a spherical shape with an average diameter around 60 nm: consistent measurements of the

average diameter were achieved with atomic force microscopy (AFM) and Scanning Electron Microscopy (SEM) (Figures 1C, 1D), which provided the value of 60 ± 15 nm and 63 ± 13 nm, respectively. In addition, with photon correlation spectroscopy, the value of 64.6 ± 0.2 nm (five measurements; see Methods section) for the hydrodynamic diameter was measured. The ammonium group loading, available for the interaction with the MB, was determined by potentiometric titration of the bromide and chloride ions obtained after complete ion exchange followed by titration with a 0.0201 M solution of $AgNO_3$ and was found to be 370 μmol of quaternary ammonium bromides and 185 μmol of primary ammonium chlorides per gram of NPs (Figure 1B and Materials and Methods section for details). The use of fluorescein as di-allyl derivative (see Materials and Methods) allows the incorporation of the fluorophore through a stable covalent bond within the PMMA core. Finally, the ζ-potential of NPs (34.3 mV), which was measured after dialysis and ultrafiltration purification, confirmed that the cationic co-monomer employed in the polymerization reaction is covalently bound to the nanoparticle surface, demonstrating together with the argentometric titration the presence of the ammonium salts in the shell of the nanoparticles.

Figure 1 here

In view of the possible exploitation of the fluorescence of the NPs as reference signal to verify their uptake by the cells, a characterization of the NPs fluorescence at different pH was conducted in order to exclude any possible fluorescence variation due to NPs localization in cell compartments characterized by different acidic environments. NPs at an initial concentration of 10.1 $mg.mL^{-1}$ were diluted 1:500 in citrate/phosphate buffers (McIlvaine's Buffer System) at pH 8, 5.6 and 2 and fluorescence was measured in cuvette with the setup described in the "Materials and Methods" section. As shown in Figure S1A, the fluorescence of the NPs used in this work, where the fluorescein is covalently bound to the PMMA core, is characterized by a low variation at different pH values. On the other hand, when carrying out the same experiments with analogues PMMA-NPs, which incorporate fluorescein by bare

hydrophobic interactions, a nearly complete loss of emission at very low pH is observed (Figure S1B).

3.2. Survivin-directed MB characterization in solution

The sequence of the selected survivin mRNA-specific MB has been published in 2004 (Nitin et al., 2004), and it was designed on a region of the human survivin mRNA conserved among the sequences available in GenBank (Accession numbers: HM625836.1; NM_001168.2; NM_001012270.1; NM_001012271.1). A central region composed of fifteen deoxynucleotides, which is the specific sequence for survivin mRNA binding, forms the MB loop and five complementary deoxynucleotides at the 5' and at the 3' ends form the stem. The thirty deoxynucleotide DNA target, used to represent survivin mRNA, is composed of a region specific to this sequence plus other deoxynucleotides not-specific for the stem sequence of the MB but contained in survivin mRNA. The MB makes use of ATTO 647N (λ_{abs} 644 nm, λ_{em} 669 nm) and Blackberry Quencher 650 (BBQ650) (λ_{max} ~ 650 nm, useful absorbance between 550 and 750 nm) as fluorophore/quencher pair (see Materials and Methods for details). The non-specific sequence has a consensus of eight not-consecutive deoxynucleotides with the target. The reverse MB has a complete reverse sequence with respect to the survivin mRNA-specific MB.

Survivin MB was initially evaluated in solution, since one might expect a diverse behaviour in samples with different analytical characteristics. More precisely, the MB-target binding ability was evaluated under different buffer conditions, by using three standard buffers, characterized by different pH and salt composition: Tris 10 mM pH 8 with the addition of 10 mM MgCl2, phosphate buffer saline (PBS) 15 mM pH 7.4 and HEPES 20 mM pH 7.2. The MB (100 nM) and its specific target at different concentrations (from 0 nM to 1 µM) were incubated in the different buffers for 1 h. Afterwards, fluorescence was acquired by exciting at 635 nm with an integration time of 1 sec. In order to compare the different measurement

settings, the fluorescence intensity (F) averaged between 640 nm and 700 nm (the wavelength band containing the maximum of the fluorophore emission) obtained for each target concentration, was normalized with respect to the fluorescence F_0 of the MB in buffer (Figure 2A). The activity of the MB in the three considered buffers was similar except for an evident higher F/F_0 at lower target concentrations in Tris 10 mM pH 8 with the addition of 10 mM $MgCl_2$, which confirmed the importance of Mg^{2+} cations for MB folding (Kuhn et al., 2002).

The specificity of the MB interaction was examined by measuring the fluorescence of the MB incubated with i) a non-specific sequence, ii) with its target and iii) by incubating the reverse MB with the MB target (all experiments were conducted using a 100 nM MB concentration). Notably, the higher signal to buffer ratio was observed for the MB interacting with its target (7.5-fold increase) with respect to the increase after interaction with the non-specific sequence (1.3-fold increase) or to the signal of the reverse MB with the MB target (1.1-fold increase), thus confirming the strong specificity of the MB for the selected target (Figure S2).

3.3. MB loaded onto PMMA-NPs: characterization in solution

A549 cells in RPMI 1640 culture medium supplemented with 10% Fetal Bovine Serum (FBS) represent the human cancer cell model used in this work for the studies of the cellular uptake of the MB loaded onto the PMMA-NPs (MB@PMMA-NPs).

On the basis of the results described in the previous section which testified for a dependence of the MB binding ability on the environment, such as the used buffer, the functionality of the free MBs and of the MB@PMMA-NPs was evaluated in culture medium. The fluorescence intensity of the MB (100 nM) incubated with the target (100 nM) in culture medium, displayed a 3.1 times increase after 90 min incubation time with respect to the free MB after the same incubation time (blue and red curves, respectively, in Figure 2B), confirming the ability of the MB to open its hairpin structure in the presence of its target. The fact that the fluorescence of the free MB is subject to only 1.1 fold increase after 90 minutes of incubation

in the absence of the target (red curve in Figure 2B) also proves that the fluorescence increase is almost exclusively due to the binding to the target and not to the presence of interfering substances, which compose the medium.

Similar measurements were performed using the MB@PMMA-NPs nano-complex obtained right before adding the target, by simple mixing for 3 minutes of 100 nM MB with 10 µg mL-1 of PMMA-NPs (Figure 2C) in the used culture medium, which results in the electrostatic interaction of the negatively charged MB with the positively charged PMMA-NPs shell. The results obtained after 90 min incubation time with the target showed a fluorescence of the MB@PMMA-NPs, 2.1 times higher than the fluorescence in the absence of the target (blue and red curves, respectively, in Figure 2C). The 90 minutes of incubation in the absence of the target implies only a fluorescence increase of a factor 1.1 (with respect to the free MB at time 0, red and green curves, respectively, in Figure 2C). However, when the MB is loaded onto the nanoparticles, a lower fluorescence increase, upon the incubation with the target, was observed with respect to the MB without nanoparticles (2.1 *versus* 3.1). This might be due to the partial hampering of the MB hairpin structure opening and/or of the interaction with the target after the adsorption of the MB onto the NPs. Moreover, the high MB density on the NPs could reduce its binding efficiency to the target as widely recognized and demonstrated for probes covalently immobilized (Situma et al., 2007; Vainrub and Pettitt, 2003). In addition, a decrease of target molecules available for the binding with the MB can also arise from their electrostatic adsorption onto the positively charged NPs (Cederquist and Keating, 2010) leading to a decrease in fluorescence.

In order to further characterize the MB@PMMA-NPs ability to interact with the target in the cell culture medium, the fluorescence intensity was evaluated at different concentrations of the target (0, 1, 10, 100 nM) and at different incubation times (0, 90, 180 min) (Figure 2D).

An increase of fluorescence was observed at increasing concentrations of target and incubation times.

Figure 2 here

3.4. Effects of PMMA-NPs on the A549 cell viability

The effect of different concentrations of PMMA-NPs on A549 cells viability was evaluated by WST-1 assay as reported in the Material and Methods (Supplementary material section). Remarkably, no significant effect on cells viability was observed after 60 and 180 min of incubation, except for the highest tested concentration, 50 µg/mL, which gives a negligible decrease (Figure S3A-B).

Despite higher concentrations resulted as not toxic by WST-1 assay, concentrations above 10 µg mL-1 were not considered for the subsequent experiments, since confocal fluorescence imaging analysis revealed a slight morphological alteration of the cells and the concomitant formation of a non-transparent coating on their surface. On the other hand, concentrations below 10 µg mL^{-1} were excluded because they provided barely visible fluorescence signals. Consequently, on the basis of cells viability results and in order to guarantee the visualization of measurable fluorescent signals, the 10 µg mL-1 PMMA-NPs concentration was chosen for the cellular localization studies performed by confocal microscopy.

In this experimental model, the survivin mRNA expression was also evaluated. Survivin mRNA expression was clearly evident in A549 cells, as shown by the electrophoretic band of its cDNA compared to that of the housekeeping gene β-actin, obtained after RT-PCR amplification (Figure S3C).

3.5. PMMA-NP cellular uptake

The incubation of A549 cells with PMMA-NPs was realized in RPMI 1640 medium supplemented with 10% FBS at different times of exposure (from 10 min up to 48 h).

FBS, which could promote the formation of NPs aggregates, was added to the culture medium because its presence ensures the proper physiological activity of the cell membrane, which is

an essential requirement for uptake studies, while allowing performing long-term studies because of the healthy conditions of the cells.

As reported in figure 3A, after 10 min of incubation, PMMA-NPs were scattered on the plasma membrane; after 60 min of incubation, they were predominantly on the plasma membrane and larger aggregates could be localized on the intracellular side of the plasma membrane (Figure 3B). Instead, after 90 min of incubation, clusters of NPs were clearly detectable inside the cell (Figure 3C). These results are in accordance with previously reported data on other human tumour cell lines (Duchi et al., 2013; Mastrobattista et al., 2006).

Figure 3 here

For more prolonged exposure times, 3 h and 13 h, as shown in figure S4A and B, the nanoparticles were still inside the cells where they remained as aggregates also after 48 h of incubation (data not shown).

Collectively these results allowed identifying 90 min as the right incubation time for NPs internalization into A549 lung adenocarcinoma cells in the chosen experimental conditions. Thus, the experiments with free MB and the MB loaded onto PMMA-NPs were realized with this incubation time.

3.6. MB@PMMA-NP cellular uptake studies

Images of A549 cells incubated for 90 min with 2 mL MB@PMMA-NPs, at a final concentration of 100 nM MB and 10 µg mL-1 PMMA-NPs, are shown in figure 4A and 4B.

Magnified green, red and merged images of the cell selected in figure 4A are displayed in figure 4D, 4E and 4C, respectively. Both green and red spots are inside the cell, as observed in XZ and YZ projections of the image stacks.

Figure 4 here

In order to assess the MB signal in the absence of PMMA-NPs, A549 cells were incubated also with the MB alone.

Figure 5 shows the transmission and fluorescence images of A549 cells treated with 100 nM MB alone for 90 min in complete medium.

Figure 5 here

Unspecific opening of few MB molecules and/or incomplete quenching might account for the detectable signal. In order to quantify the effects of PMMA-NP incubation, particle analysis was carried out on thresholded equatorial XY images of cells treated with MB alone (20 cells) or with MB@PMMA-NPs (20 cells). The first group of cells displayed a mean number of particles per cell of 1.90 ± 0.40 with a mean area of 1.04 ± 0.20 μm^2, while in the second group the analysis identified 27.50 ± 2.30 particles per cell with a mean area of 2.35 ± 0.16 μm^2. The means are statistically different ($p < 0.001$, Student t test).

These results are in agreement with literature data, which report that RNAs, ssDNA/dsDNAs cannot be effectively internalized by cells without using a carrier or a specific transfection agent (Adinolfi et al., 2015; Duchi et al., 2013). Moreover, results show that, in our experimental conditions, PMMA-NPs promote a clear-cut MB uptake.

The co-localization of the fluorescence signals of PMMA-NPs and MB (Figure 4C) is partial (Pearson's index of 0.2), indicating that the PMMA-NPs, which are effective in promoting the MB uptake, do not follow the same fate of MB inside the cell. This partial co-localization could be due to the dissociation of the MB from the PMMA-NPs once internalized into the cell or in proximity of the mRNA target.

In perspective of a future *in vivo* application, we wanted to evaluate the effect of MB@PMMA-NPs on healthy cells. As healthy control, Human Dermal Fibroblasts from adult (HDFa) were chosen in agreement with what previously demonstrated by Adinolfi et al, 2015. Under the same experimental conditions used in this study for A549 cells for the MB@PMMA-NPs, the fibroblasts (Figure 6A), while internalizing the PMMA-NPs, as demonstrated by the fluorescence displayed exciting at 488 nm (Figure 6B), do not show a detectable labeling of survivin mRNA (Figure 6C). These data confirm the specificity of the survivin MB, not only in solution where a negligible non-specific opening was observed, but also in a more complex system, such as living cells.

Figure 6 here

4. Conclusions

The herein described core-shell polymethylmethacrylate nanoparticles have been synthesized through a versatile and very effective in-water emulsion co-polymerization reaction, that allows to access a large number of multi-functionalized polymeric nanoparticles by simply changing the co-monomers and the reaction parameters. In particular, we reported here about highly fluorescent 60 nm nanoparticles, which display an external shell decorated with quaternary ammonium groups available for electrostatic loading of negatively charged MB. Additionally, the remaining primary ammonium groups could be efficiently exploited for further covalent functionalization with drugs, pro-drugs, or other biologically active compounds.

The characterization of the MB in solution revealed a good specificity and sensitivity, confirmed also after its adsorption onto the PMMA-NPs.

The results obtained by confocal microscopy in cancer cells and those found in HDFa, demonstrated that the PMMA-NPs efficiently promote the MB internalization generating a

specific fluorescent signal in the presence of survivin mRNA expression, paving the way to a semi-quantitative real time evaluation of the survivin expression. These evidences highlight that the use of 10 µg mL^{-1} PMMA-NPs as carrier for survivin-directed MB for 90 min might be a promising strategy to reduce cancer cell proliferation avoiding detectable consequences on healthy cells.

Acknowledgements

This work was supported by the national flagship project Nanomax. The authors wish to thanks C. Domenici (IFC-CNR, Pisa, Italy) for the fruitful discussion.
Sara Tombelli thanks the European Community for the project Nanodem - NANOphotonic Device for Multiple therapeutic drug monitoring (FP7 - 8318372).

References

Adinolfi, B., Pellegrino, M., Baldini, F., 2015. Biomed. Pharmacother. 69, 228-232. doi: 10.1016/j.biopha.2014.12.003.

Ashley, C.E., Carnes, E.C., Epler, K.E., Padilla, D.P., Phillips, G.K., Castillo, R.E., Wilkinson, D.C., Wilkinson, B.S., Burgard, C.A., Kalinich, R.M., Townson, J.L., Chackerian, B., Willman, C.L., Peabody, D.S., Wharton, W., Brinker, C.J. 2012. ACS Nano 6, 2174.

Baran, M., Möllers, L.N., Andersson, S., Jonsson, I.M., Ekwall, A.K., Bjersing, J., Tarkowski, A., Bokarewa, M.J., 2009. Cell. Mol. Med. 13, 3797-3808. doi: 10.1111/j.1582-4934.2009.00721.x.

Becker, A.L., Orlotti, N.I., Folini, M., Cavalieri, F., Zelikin, A.N., Johnston, A.P., Zaffaroni, N., Caruso, F., 2011. ACS Nano. 5, 1335-1344. doi: 10.1021/nn103044z.

Bettencourt, A., Almeida, A.J., 2012. J. Microencapsul. 29, 353-367. doi: 10.3109/02652048.2011.651500.

Bishop, C.J., Kozielski, K.L., Green, J.J., 2015. J. Control Release. 219, 488-499. doi: 10.1016/j.jconrel.2015.09.046.

Biswas, S., Torchilin, V.P., 2014. Adv Drug Deliv Rev. 66, 26. doi: 10.1016/j.addr.2013.11.004.

Bogart, L.K., Pourroy, G., Murphy, C.J., Puntes, V., Pellegrino, T., Rosenblum, D., Peer, D., Levy, R., 2014. ACS Nano. 8, 3107.

Brun, S.N., Markant, S.L., Esparza, L.A., Garcia, G., Terry, D., Huang, J.M., Pavlyukov, M.S., Li, X.N., Grant, G.A., Crawford, J.R., Levy, M.L., Conway, E.M., Smith, L.H., Nakano, I., Berezov, A., Greene, M.I., Wang, Q., Wechsler-Reya, R.J., 2015. Oncogene 34, 3770. doi: 10.1038/onc.2014.304.

Carpi, S., Fogli, S., Giannetti, A., Adinolfi, B., Tombelli, S., Da Pozzo, E., Vanni, A., Martinotti, E., Martini, C., Breschi, M.C., Pellegrino, M., Nieri, P., Baldini, F., 2014. PlosOne 9, e114588. doi: 10.1371/journal.pone.0114588.

Cederquist, K.B. and Keating, C.D., 2010. Langmuir 26, 18273–18280.

Chaudhuri, R.G. and Paria, S., 2012. Chem. Rev. 112, 2373–2433.

Chen, P., Wang, Z., Zong, S., Zhu, D., Chen, H., Zhang, Y., Wu, L., Cui Y., 2016. Biosens Bioelectron. 75, 446-451.

Dalby, B., Cates, S., Harris, A., Ohki, E.C., Tilkins, M.L., Price, P.J., Ciccarone, V.C., 2004. Methods. 33, 95-103.

Dallaglio, K., Marconi, A., Pincelli, C., 2012. J. Invest. Dermatol. 132, 18. doi: 10.1038/jid.2011.279.

Duchi, S., Sotgiu, G., Lucarelli, E., Ballestri, M., Dozza, B., Santi, S., Guerrini, A., Dambruoso, P., Giannini, S., Donati, D., Ferroni, C., Varchi, G., 2013. J. Control Release 168, 225-237. doi: 10.1016/j.jconrel.2013.03.012.

Falzarano, M.S., Bassi, E., Passarelli, C., Braghetta, P., Ferlini, A., 2014. Hum. Gene Ther. 25, 927. doi: 10.1089/hum.2014.073.

Ferlini, A., Sabatelli, P., Fabris, M., Bassi, E., Falzarano, S., Vattemi, G., Perrone, D., Gualandi, F., Maraldi, N.M., Merlini, L., Sparnacci, K., Laus, M., Caputo, A., Bonaldo, P., Braghetta, P., Rimessi, P., 2010. Gene Ther. 17, 432. doi: 10.1038/gt.2009.145.

Fraix, A., Manet, I., Ballestri, M., Guerrini, A., Dambruoso, P., Sotgiu, G., Varchi, G., Camerin, M., Coppellotti, O., Sortino, S., 2015. J. Mater. Chem. B. 3, 3001. doi: 10.1039/C5TB00234.

Frohlich, E., 2012. Int. J. Nanomedicine 5577. doi: 10.2147/IJN.S36111.

Fukuda, S., Pelus, L.M., 2006. Mol. Cancer Ther. 5, 1087-1098.

Giannetti, A., Tombelli, S., Baldini F., 2013. Anal. Bioanal. Chem. 405, 6181-6196.

Guo, Y., Shao, Y., Chen, J., Xu, S., Zhang, X., Liu, H., 2016. Exp Ther Med. 11, 1847-1852.

Guo, Y., Wang, D., Song, Q., Wu, T., Zhuang, X., Bao, Y., Kong, M., Qi, Y., Tan, S., Zhang, Z., 2015. ACS Nano. 9, 6918. doi: 10.1021/acsnano.5b01042.

Hardy, N., Viola, H.M., Johnstone, V.P., Clemons, T.D., Cserne Szappanos, H., Singh, R., Smith, N.M., Iyer, K.S., Hool, L.C., 2015. ACS Nano. 9, 279. doi: 10.1021/nn5061404.

Huang, Y., Hu, F., Zhao, R., Zhang, G., Yang, H., Zhang, D., 2014. Chemistry. 20, 158-164.

Kejlová, K., Kašpárková, V., Krsek, D., Jírová, D., Kolářová, H., Dvořáková, M., Tománková, K., Mikulcová, V., 2015. .Int. J. Pharm. S0378-5173, 30292. doi: 10.1016/j.ijpharm.2015.10.024.

Kim, J., Lee, Y.M., Kang, Y., Kim, W.J. 2014. ACS Nano 8, 9358. doi: 10.1021/nn503349g.

Kobayashi, H., Turkbey, B., Watanabe, R., Choyke, P.L., 2014. Bioconjug Chem. 25, 2093. doi: 10.1021/bc500481x.

Kuhn, H., Demidov, V.V., Coull, J.M., Fiandaca, M.J., Gildea, B.D., Frank-Kamenetskii, M.D., 2002. J. Am. Chem. Soc. 124, 1097-1103.

Kumar, S., Kumar, V.B., Paik, P. 2013. J. of Nanoparticles, 2013, Article ID 672059, 24 pages http://dx.doi.org/10.1155/2013/672059.

Lee, K.D., Choi, S.H., Kim, D.H., Lee, H.Y., Choi, K.C. 2014. Arch Pharm Res. 37, 1546. doi: 10.1007/s12272-014-0489-z.

Li, J.J., Kawazoe, N., Chen, G., 2015. Biomaterials 54, 226. doi: 10.1016/j.biomaterials.2015.03.001.

Li, X., Deng, D., Xue, J., Qu, L., Achilefu, S., Gu, Y., 2014. Biosens Bioelectron. 61, 512-518.

Liu, Y.B., Gao, X., Deeb, D., Brigolin, C., Zhang, Y., Shaw, J., Pindolia, K., Gautam, S.C., 2014. Int. J. Oncol. 45, 1735-1741. doi: 10.3892/ijo.2014.2561.

Lou, P-J., Cheng, W-F., Chung, Y-C., Cheng, C-Y., Chiu, L-H., Young, T-H., 2007. J. Biomedical Materials Research. Part A, 849.

Mastrobattista, E., Van Der Aa, M.A., Hennink, W.E., Crommelin, D.J., 2006. Nat. Rev. Drug Discov. 5, 115-121.

Maurizi, L., Papa, A.L., Dumont, L., Bouyer, F., Walker, P., Vandroux, D., Millot, N. 2015. J. Biomed. Nanotechnol. 11, 126.

Mera, S., Magnusson, M., Tarkowski, A., Bokarewa, M., 2008. J. Leukoc. Biol. 83, 149-155.

Monasterolo, C., Ballestri, M., Sotgiu, G., Guerrini, A., Dambruoso, P., Sparnacci, K. Laus, M., De Cesare, M., Pistone, A., Beretta, G.L., Zunino, F., Benfenati, V., Varchi, G., 2012. Bioorg. Med. Chem. 20, 6640. doi: 10.1016/j.bmc.2012.09.023.

Nitin, N., Santangelo, P.J., Kim, G., Nie, S., Bao, G., 2004. Nucleic Acids Res. 32, e58.

Rawat, J., Gadgil, M. 2016. Cytotechnology. Apr 29.

Rimessi, P., Sabatelli, P., Fabris, M., Braghetta, P., Bassi, E., Spitali, P., Vattemi, G., Tomelleri, G., Mari, L., Perrone, D., Medici, A., Neri, M., Bovolenta, M., Martoni, E., Maraldi, N.M., Gualandi, F., Merlini, L., Ballestri, M., Tondelli, L., Sparnacci, K., Bonaldo, P., Caputo, A., Laus, M., Ferlini, A., 2009. Mol. Ther. 17, 820-827. doi: 10.1038/mt.2009.8.

Saengkrit, N., Sanitrum, P., Woramongkolchai, N., Saesoo, S., Pimpha, N., Chaleawlert-Umpon, S., Tencomnao, T., Puttipipatkhachorn, S., 2012. Carbohydr. Polym. 90, 1323-1329. doi: 10.1016/j.carbpol.2012.06.079.

Samal, S.K., Dash, M., Van Vlierberghe, S., Kaplan, D.L., Chiellini, E., Van Blitterswijk, C., Moroni, L., Dubruel, P. 2012. Chem. Soc. Rev. 41, 7147–7194.

Santangelo, P., Nitin, N., Bao, G., 2006. Ann. Biomed. Eng. 34, 39-50.

Schmidt, S.M., Schag, K., Müller, M.R., Weck, M.M., Appel, S., Kanz, L., Grünebach, F., Brossart, P., 2003. Blood 102, 571-576.

Singh, N., Krishnakumar, S., Kanwar, R.K., Cheung, C.H., Kanwar, J.R., 2015. Drug Discov. Today. 20, 578-587. doi: 10.1016/j.drudis.2014.11.013.

Situmaa, C., Moehringc, A.J., Noorc, M.A.F., Sopera, S.A., 2007. Analytical Biochemistry 363, 35–45.

Sommer, K.W., Schamberger, C.J., Schmidt, G.E., Sasgary, S., Cerni, C., 2003. Oncogene 22, 4266-4280.

Sun, T., Zhang, Y. S., Pang, B., Hyun, D.C., Yang, M., Xia, Y., 2014. Angew Chem. Int. Ed Engl. 53, 12320. doi: 10.1002/anie.201403036.

Tay, C.Y., Yuan, L., Leong, D.T. 2015. ACS Nano. 9, 5609–5617.

Teagle, A.R., Birchall, J.C., Hargest, R., 2016. Skin Pharmacol. Physiol. 29, 119-129.

Teo, P.Y., Cheng, W., Hedrick, J.L., Yang, Y.Y., 2015. Adv. Drug Deliv. Rev. pii: S0169-409X(15)00239-2. doi: 10.1016/j.addr.2015.10.014.

Tian, J., Luo, Y., Huang, L., Feng, Y., Ju, H., Yu, B.Y., 2016. Biosens Bioelectron. 80, 519-524. doi: 10.1016/j.bios.2016.02.018.

Vainrub, A., Pettitt, B.M., 2003. Biopolymers 68, 265–270.

Varchi, G., Benfenati, V., Pistone, A., Ballestri, M., Sotgiu, M., Guerrini, A., Dambruoso, P., Liscio, A., Ventura, B., 2013. Photochem. Photobiol. Sci., 12, 760–769.

Varchi, G., Foglietta, F., Canaparo, R., Ballestri, M., Arena, F., Sotgiu, G., Guerrini, A., Nanni, C., Cicoria, G., Cravotto, G., Fanti, S., Serpe, L., 2015. Nanomedicine. 10, 3483. doi: 10.2217/nnm.15.150.

Varchi, G., Foglietta, F., Canaparo, R., Ballestri, M., Arena, F., Sotgiu, G., Guerrini, A., Nanni, C., Cicoria, G., Cravotto, G., Fanti, S., Serpe, S., 2015. Nanomedicine, 10, 3483–3494.

Wang, J., Zhu, R., Sun, X., Zhu, Y., Liu, H., Wang, S.L. 2014. Int J Nanomedicine 9, 3987. doi: 10.2147/IJN.S64103.

Wang, Q., Chen, L., Long, Y., Tian, H., Wu, J., 2013. Theranostics 3, 395-408.

Wang, Y., Gao, S., Ye, W.H., Yoon, H.S., Yang, Y.-Y., 2006. Nat. Mater.5, 791.

Wu, Y.K., Huang, C.Y., Yang, M.C., Lan, C.C., Lee, C.H., Chan, E.C., Chen, K.T., 2014. Med. Oncol. 31, 79. doi: 10.1007/s12032-014-0079-4.

Zhang, X.S., Huang, J., Zhan, C.Q., Chen, J., Li, T., Kaye, A.D., Wu, S.X., Xiao, L., 2016. Pain Physician 19, 189-196.

Zheng, J., Yang, R., Shi, M., Wu, C., Fang, X., Li, Y., Li, J., Tan, W., 2015. Chem. Soc. Rev. 44, 3036-3055. doi: 10.1039/c5cs00020c.

Figure 1

Click here to download high resolution image

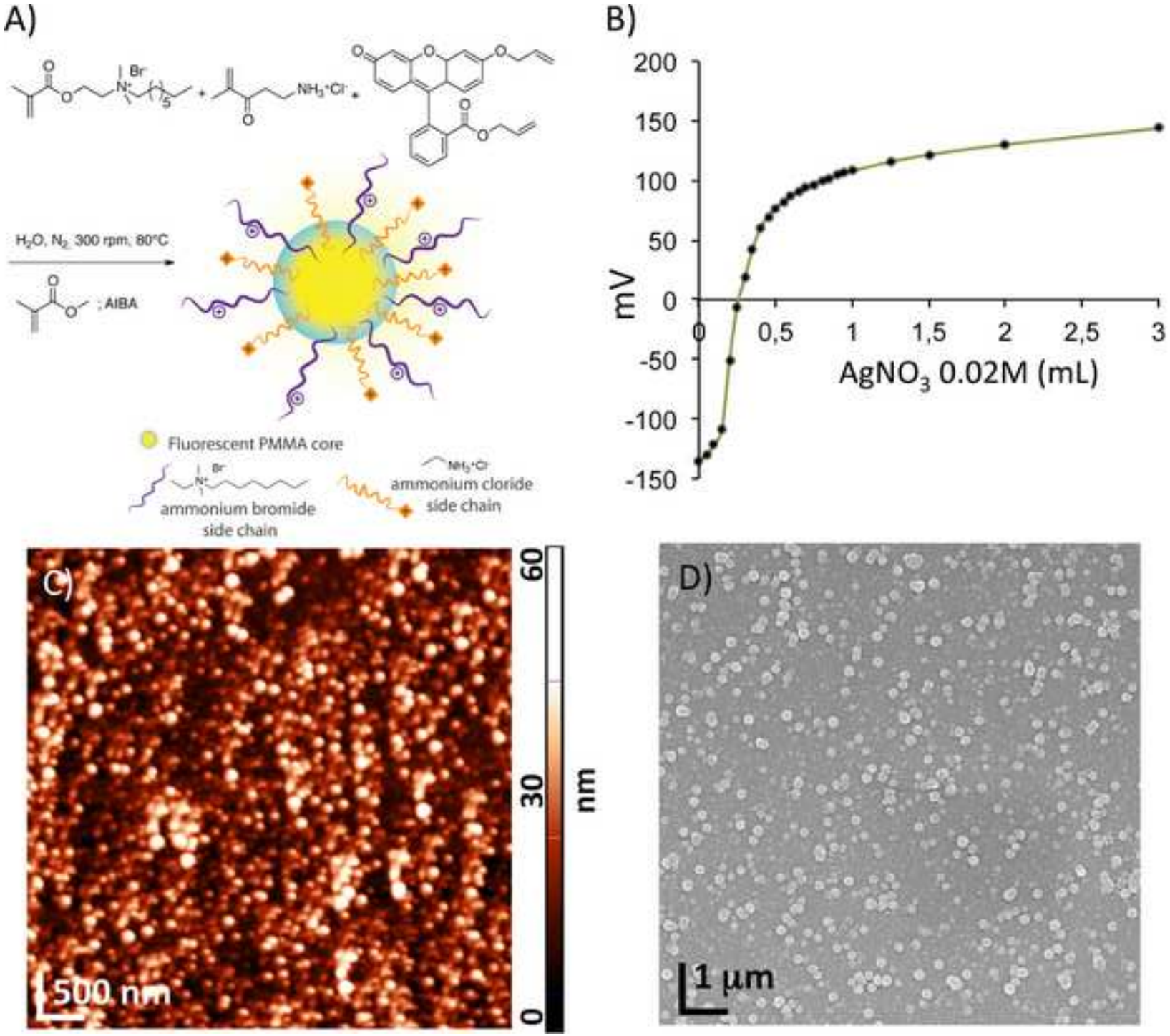

Figure 2 revised

Click here to download high resolution image

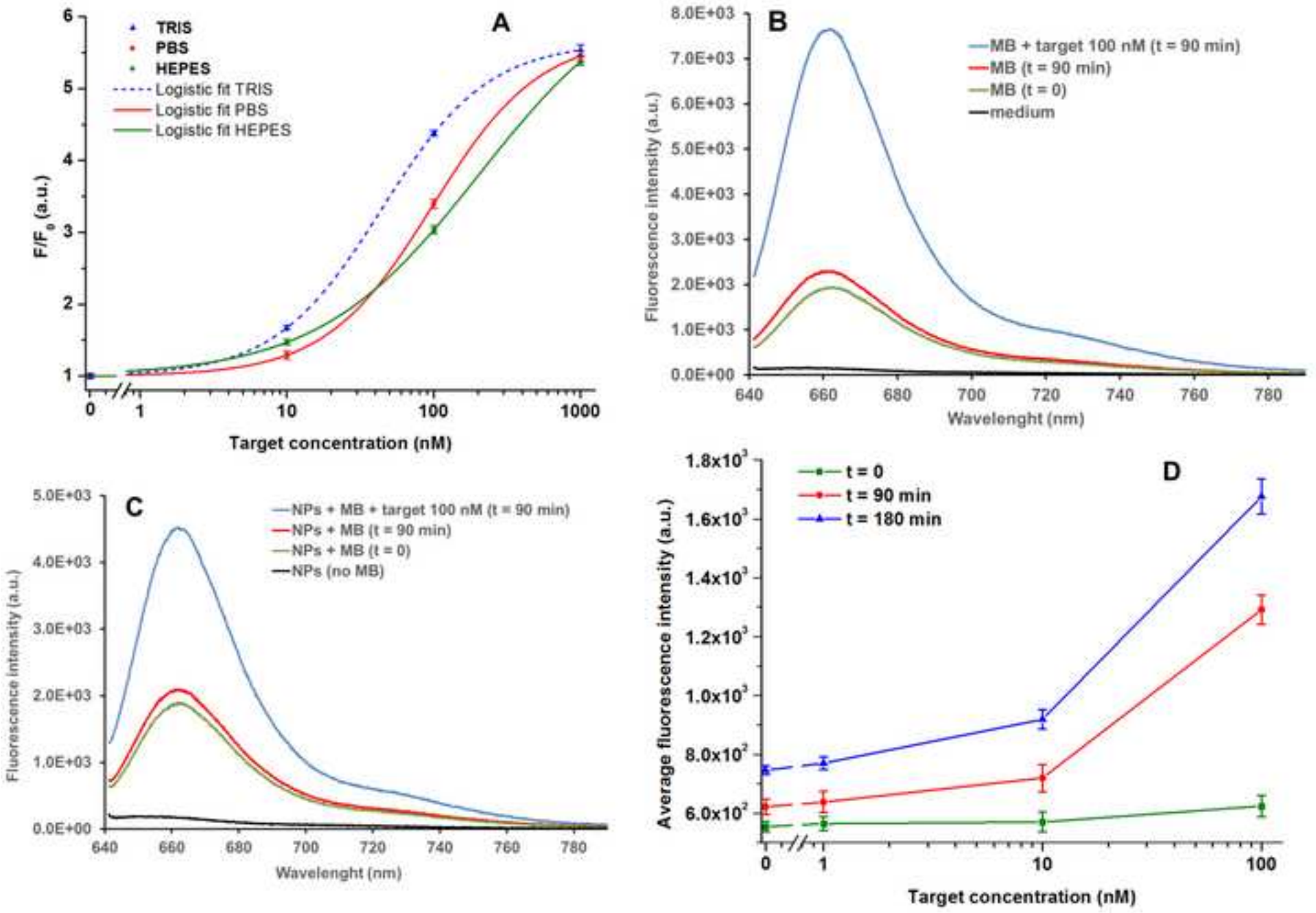

Figure 3

Click here to download high resolution image

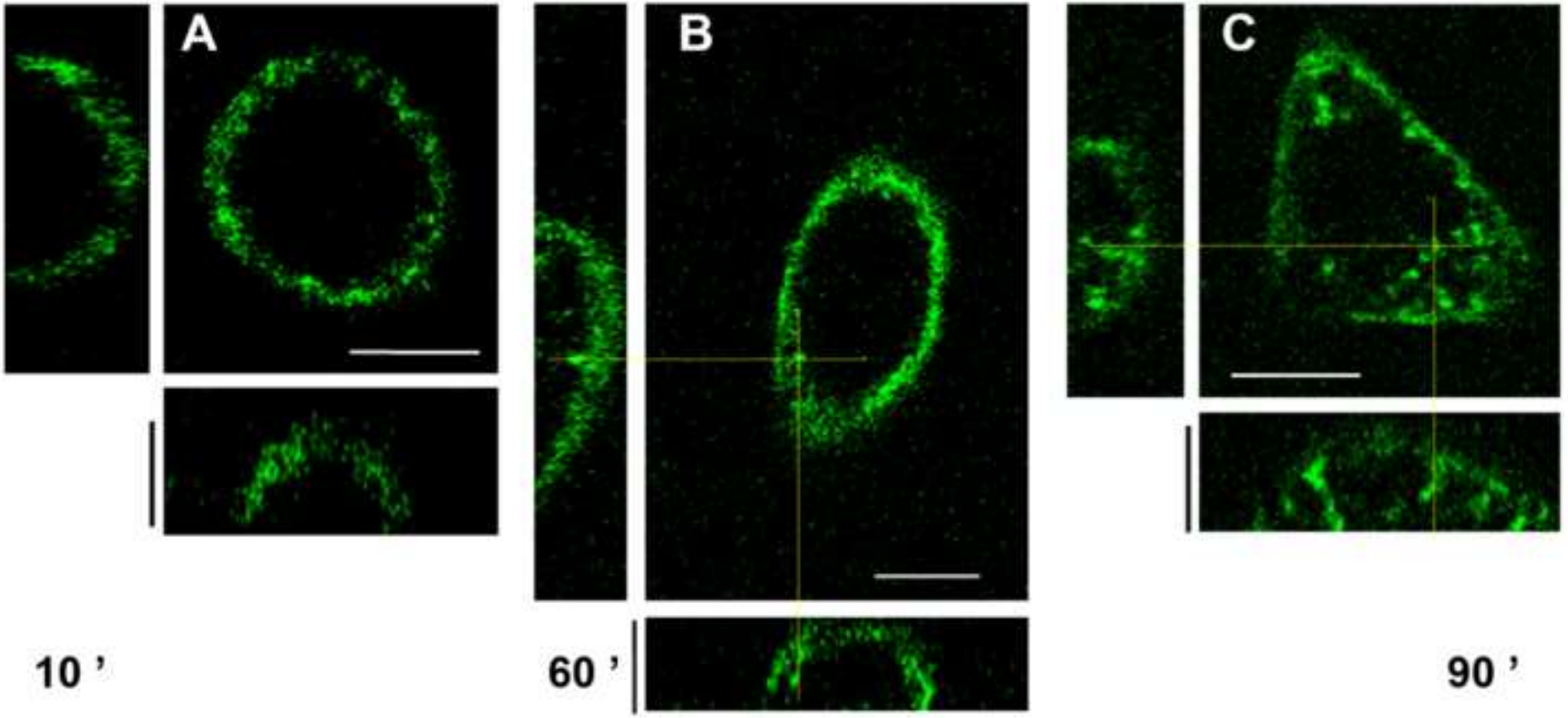

Figure 4

Click here to download high resolution image

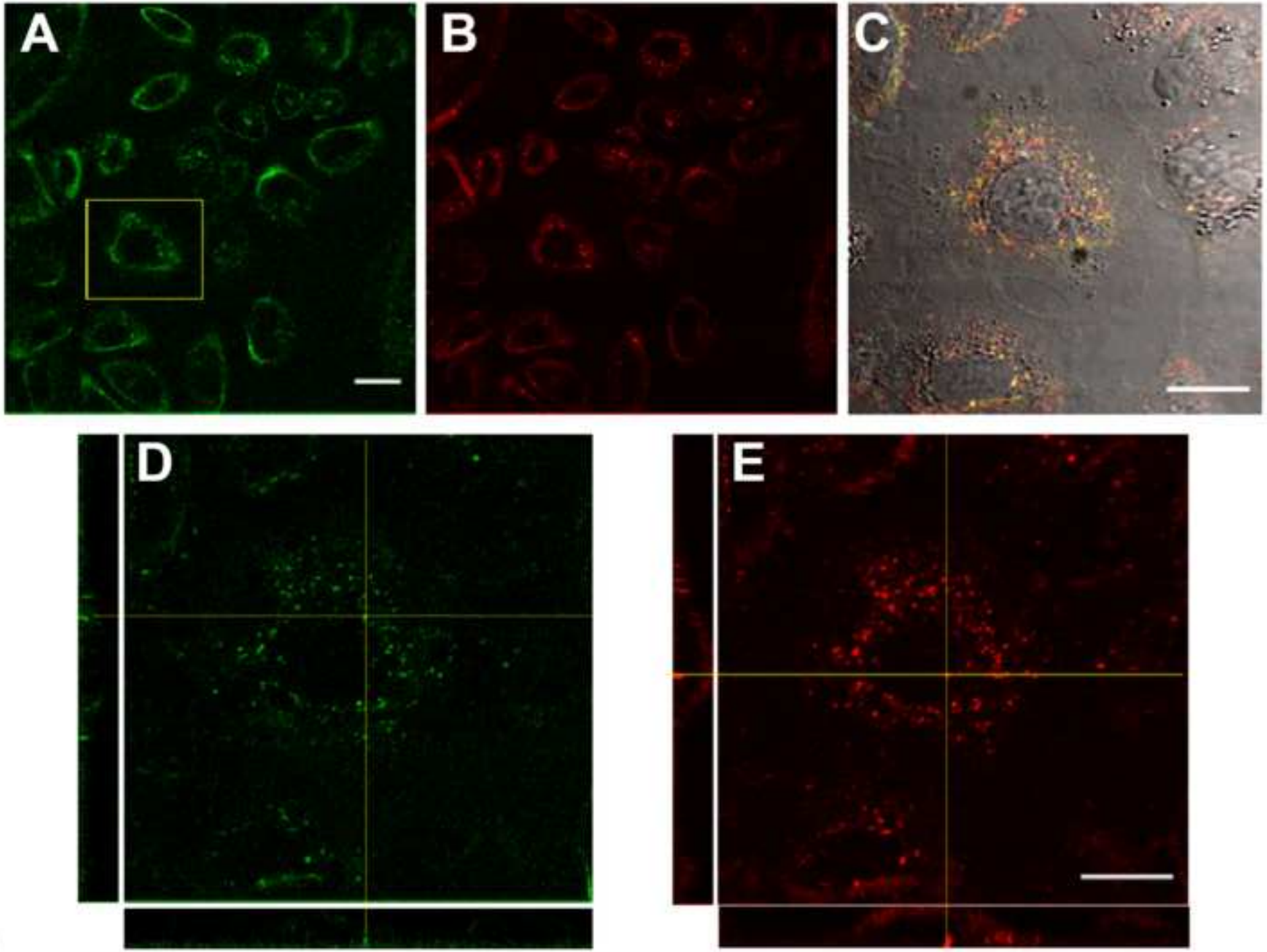

Figure 5

Click here to download high resolution image

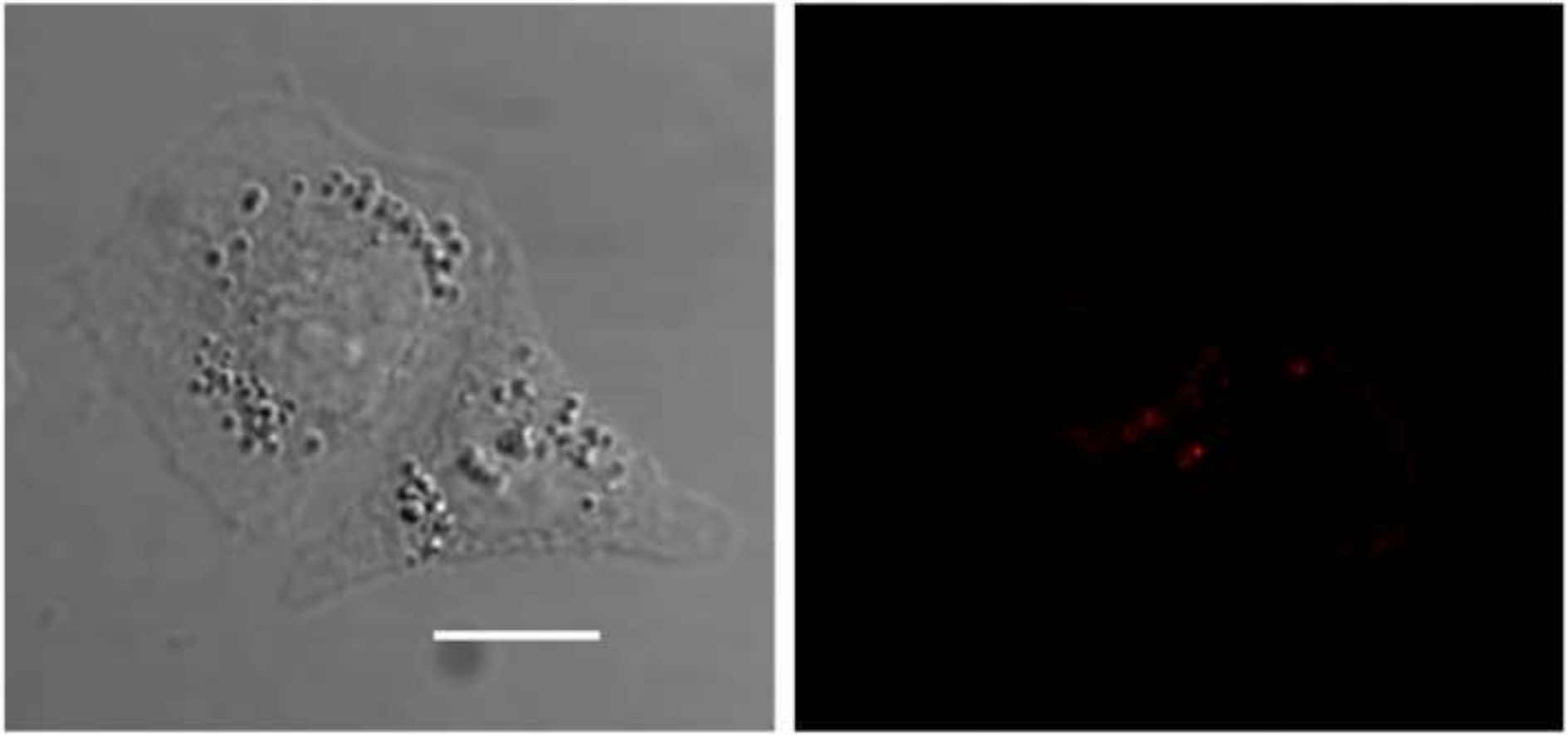

Figure 6

Click here to download high resolution image

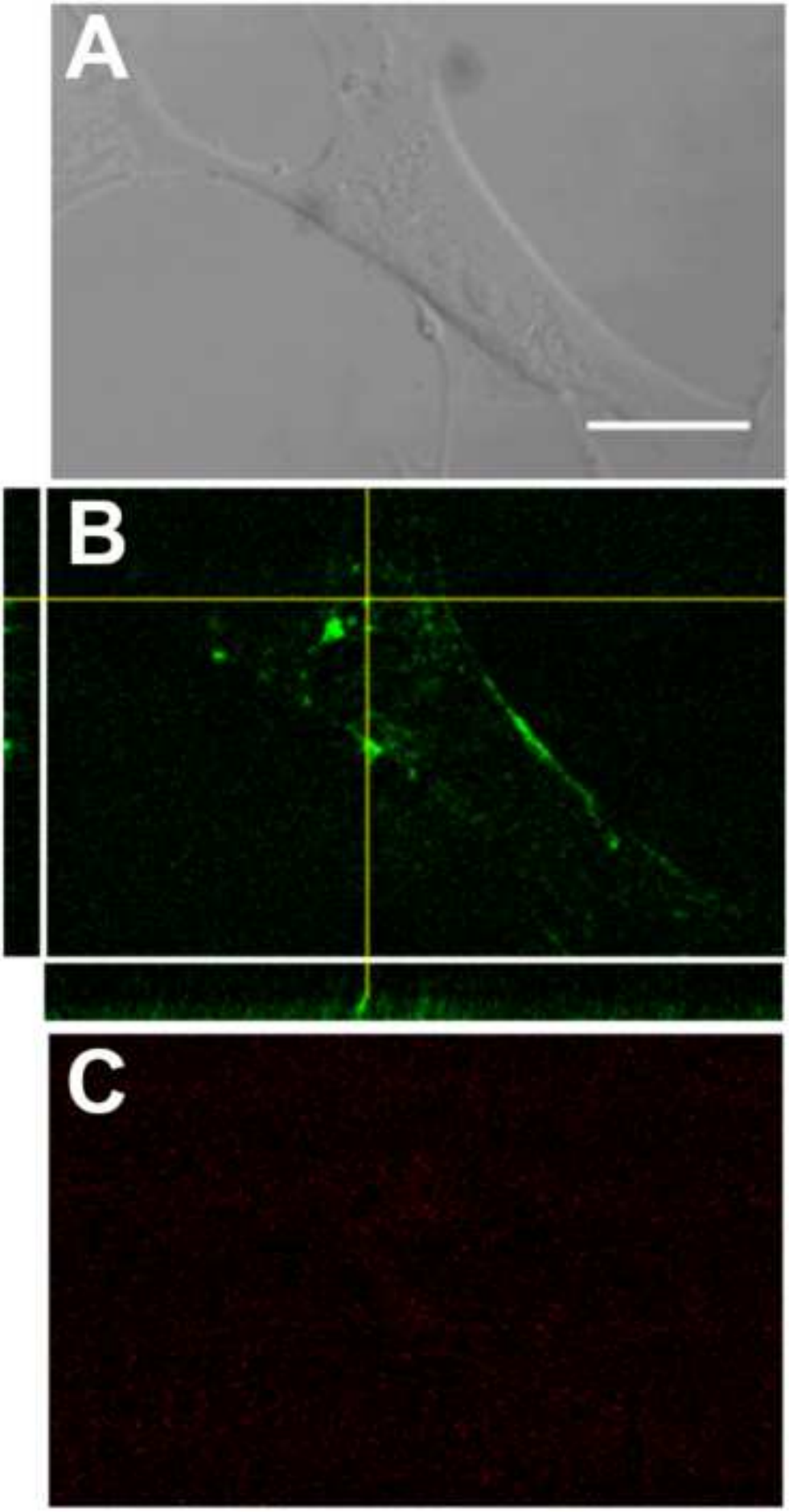

Figure captions

Figure 1. A) Synthesis of core-shell PMMA-NPs; B) PMMA-NPs argentometric titration curve; C) AFM image of nanoparticles deposited on atomic flat silicon; Z-range = 60±15 nm. D) SEM image of PMMA-NPs; Z-range = 63±13 nm.

Figure 2. A) Normalized fluorescence intensity (averaged between 640 nm and 700 nm) of the MB incubated with the target at different concentrations in Tris, PBS and HEPES buffers (incubation time 1 h, integration time 1 sec, λ_{ex} 635 nm). Fitting: logistic fit ($y = A_2 + (A_1-A_2)/(1 + (x/x_0)^p)$) with three free parameters (A_2, x_0 and p) and one fixed parameter ($A_1 = 1$). B) Fluorescence spectra of the MB solution without and with target 100 nM at zero and 90 min of incubation in RPMI 1640 medium supplemented with 10% FBS (λ_{ex} 635 nm). C) Fluorescence spectra of the MB solution without and with target 100 nM at zero and 90 min of incubation in RPMI 1640 medium supplemented with 10% FBS in presence of PMMA-NPs at a concentration of 10 µg/mL (λ_{ex} 635 nm). D) Fluorescence intensity (averaged between 640 nm and 700 nm) of the molecular beacon in presence of different concentrations (0-100 nM) of the target at increasing incubation times (0, 90 and 180 minutes) in RPMI 1640 medium supplemented with 10% FBS in presence of PMMA-NPs at a concentration of 10 µg/mL (λ_{ex} 635 nm).

Figure 3. Confocal microscopy images of A549 living cells incubated with PMMA-NPs (10 µg/mL) for different times (10, 60 or 90 minutes, in A, B and C, respectively) (excitation at 488 nm). Each panel illustrates an equatorial XY image along with the relative XZ and YZ projections of the image stack. Vertical and horizontal scale bars are 15 µm.

Figure 4. Confocal microscopy images of A549 living cells incubated with 100 nM survivin MB@10 µg/mL PMMA-NPs for 90 minutes in complete medium. A) fluorescence image with excitation at 488 nm; B) fluorescence image with excitation at 638; D, E) magnification of the region of interest marked in A observed; C) merged image of the magnified region. Each panel shows an equatorial XY image and the relative XZ and YZ projections of the image stack. Transmission and fluorescence images are merged in C. Horizontal scale bars are 20 µm in A, B and 15 µm in C, D, E.

Figure 5. Confocal microscopy images of two A549 living cells incubated with 100 nM MB alone for 90 minutes, in complete medium. A) DIC transmission image; B) fluorescent image (excitation at 638 nm). Scale bar: 15 µm.

Figure 6. Confocal microscopy images of an HDFa living cell incubated with 100 nM survivin MB@10 µg/mL PMMA-NPs for 90 minutes in complete medium. A) Transmission DIC image; B) an equatorial XY image and the relative XZ and YZ projections of the image stack (excitation 488 nm); C) fluorescence image with excitation at 638 nm. Scale bar is 20 µm.